Computational Modeling of Peripheral Nerve Stimulation

Brian H. Tracey, *Member, IEEE,* Plamen Krastev, Zhixiu Han, and Michael Williams

Abstract— Nerve localization using peripheral nerve stimulation (PNS) is affected by tissue properties, the anatomy surrounding the nerve, and characteristics of the stimulus waveform. A better understanding of the factors influencing PNS should lead to improved nerve localization techniques for use in regional anesthesia. A finite element approach is described here that includes capacitive effects and accounts for frequency-dependent tissue properties in a computationally efficient manner. The modeling approach can be applied to other bioelectric problems where capacitive effects may be important.

I. INTRODUCTION

Peripheral nerve stimulation (PNS) is a widely used technique for localizing nerves in regional anesthesia [1,2]. This technique utilizes a needle which provides both electrical stimulation and drug delivery. The physician advances the needle towards the nerve to be anesthetized while electrically stimulating the nerve. Nerve excitation is typically observed by means of visible muscle twitch. When a threshold response is obtained with a low target current (typically in the range of 0.5 mA) the needle is judged to be in close proximity to the nerve and anesthetic is delivered.

The ability to localize nerves using PNS is affected by a variety of factors, including the stimulus waveform, local anatomy, and tissue properties. Because PNS is invasive, investigating these factors using computer modeling is attractive. A computer model of PNS was recently developed [1] and used to study the effects of stimulus waveform. While [1] models the tissue as a homogenous half-space, the work described here studies PNS using a finite element model (FEM). This allows the modeling of spatially varying tissue properties and realistic anatomy, which were recently hypothesized to be causes of observed variability in the stimulation currents needed to elicit muscle twitch in PNS [3]. Realistic modeling should help improve the understanding of PNS and will hopefully lead to nerve block procedures with improved safety and success rates.

The bioelectric field calculation approach used here includes several enhancements over standard bioelectric modeling. Most modeling studies make the assumption that the electrical field can be regarded as quasistatic and that capacitive effects can be neglected [4-5]. In some scenarios capacitive effects can be noticeable, for example when modeling short-duration pulses such as those used in PNS. Capacitance in biological tissues is generally frequency-dependent, giving rise to dispersion effects. These effects have been modeled using a combined time domain/frequency domain solution [5], at the cost of greater model complexity.

In many cases, both the magnitude and phase of the electrical field vary smoothly with frequency. This suggests the use of an interpolation approach in which the field equations are solved at a smaller number of frequencies, then interpolated to a set of finely spaced FFT frequency bins and inverse transformed. This approach leads to a computational savings of roughly two orders of magnitude as compared to a brute-force direct calculation. While straightforward, the interpolation approach does not appear to have been previously applied to bioelectric field modeling. A second enhancement is that the exact Helmholtz solution was used. This solution was found to be as computationally fast as approximate quasistatic solutions.

The electrical field calculated from the FEM model is used to excite a nerve model consisting of individual fibers that are described by the Frankenhaeuser-Huxley fiber model [7]. Stimulus response curves calculated for the nerve are used to predict nerve response as a function of stimulus current and needle position. Finally, an example is shown of simulating a PNS procedure.

II. METHODS

A. Bioelectric field equation

Maxwell's equations predict that the electric and magnetic fields in a media with sources satisfy the inhomogeneous wave equation. It then follows that the Fourier components of the scalar and vector potentials satisfy respectively the scalar and vector Helmholtz equations. A brief but clear derivation is given in a recent paper [6] which discusses various approximations in modeling electric fields in biological tissues. Written in terms of the complex $\sigma_c(\omega) = \sigma(\omega) + j\omega\varepsilon_r(\omega)\,\varepsilon_0$, the Helmholtz equation is

$$\sigma_c(\omega)\nabla^2\varphi - j\mu\omega\sigma_c{}^2(\omega)\varphi = \nabla \cdot J \qquad (1)$$

where σ and ε_r are the conductivity and relative permittivity of the tissue, ϕ is the potential, ε_0 is the permittivity of vacuum, μ is the magnetic permeability, and the right-hand side represents a current source (assumed below to be a point

B.H. Tracey is NeuroMetrix, Inc, Waltham, MA 02450, USA (781-314-2753; fax: 781-890-1556; e-mail: btracey@ neurometrix.com).

Z. Han is with iWalk, Inc. (e-mail: zhan@iwalkpro.com)

P. Krastev and M. Williams are also with NeuroMetrix, Inc. (e-mail: pkrastev@neurometrix.com, mwilliams@neurometrix.com).

source). As noted, the conductivity and permittivity are assumed to be functions of frequency.

Boundary conditions for the problem are φ=0 on the ground electrode, no current flowing through tissue/air surfaces, and continuity of current across internal interfaces. Together, Eq. 1 and the boundary conditions describe a problem that can be solved to give the electrical field.

Most published studies rely on simplifications of Eq. 1, typically ignoring propagation effects, tissue capacitance, and frequency-dependence of tissue properties [8]. A method for including frequency-dependent tissue properties is described in the next section. A numerical study was made of using the exact Helmholtz solution in the FEM model vs. approximate quasistatic solutions. The Helmholtz solution matched closely to a quasistatic solution that retained capacitive effects. However, the Helmholtz solution did not noticeably increase the computational load, so the exact solution is used in this paper.

B. Modeling of frequency-dependent tissue properties

A current pulse $x(t)$ is applied to stimulate the nerve. The resulting waveform in the tissue can be found using a frequency-domain solution. The current pulse is first transformed (via FFT) into the frequency domain, giving a spectrum $X(f)$. Let $g(f,R)$ be the calculated field for each frequency and spatial point, for a unit amplitude current source. The frequency-domain solution $g(f,R)$ is then weighted by $X(f)$, and is inverse transformed to find the time domain solution:

$$\varphi(t,R) = \mathfrak{I}^{-1}\big[g(f,R) \cdot X(f)\big] \qquad (2)$$

where $\mathfrak{I}^{-1}$ denotes the inverse Fourier transform. Note that $g(f,R)$ must be found for every frequency, and that accurately representing the pulse may require several thousand frequency bins.

Here, an interpolation approach is used for solving Eq. 2. The basic observation behind the interpolation approach is that the frequency-domain solution $g(f,R)$ is often a slowly varying function of frequency. It is therefore possible to find the solution at a coarse frequency spacing, then interpolate it to the FFT frequency bins. The interpolated unit-amplitude solution can be used in Eq. 2 to find the time-domain solution. If there are M bins in the coarse frequency spacing and N FFT bins, the computational savings will be on the order of N/M. Convergence is checked by refining the frequency spacing (for example, using $2M$ points) and checking for changes in the predicted time series.

Using this interpolation approach, the electrical field in the tissue was calculated for a series of needle locations of increasing depth, modeling the approach of the needle towards the nerve.

C. Nerve geometry and nerve fibers

For simulations shown here, the nerve was assumed to consist of 50 myelinated nerve fibers running parallel to the along-axis (x) dimension of the model. While peripheral nerves typically contain hundreds of fibers, the number of fibers was limited in simulation to avoid increasing the computational load too greatly (time spent computing the nerve response greatly exceeded the time spent calculating the external fields). The nerve fibers were randomly distributed inside a cylindrical nerve of 0.5 mm diameter. Fiber diameters were chosen randomly from a tri-modal distribution described by Boyd and Davy [9]. The effect of the nerve on the external electrical field was neglected.

The response of each individual nerve fiber was described using the well-known Frankenhaeuser-Huxley, or F-H model [7]. The trans-membrane voltage at the nodes of Ranvier is expressed as a matrix equation [1]:

$$c_m \frac{\partial \mathbf{V}_m}{\partial t} + i_{ion} = G\big(\mathbf{V}_m + \mathbf{V}_e\big)$$

where $\mathbf{V}_m$ are the transmembrane voltages and $\mathbf{V}_e$ are the external field values at each node. The first term on the left represents capacitive currents across the membrane, while the second represents the summed ionic currents through ion channels. These ionic currents have a complicated nonlinear behavior that is described by the F-H model. The right side represents current flow from adjacent nodes, with G being a tridiagonal matrix representing the conductance between adjacent nodes.

To reduce computational load, the number of active nodes (where the F-H equations are used to calculate i_{ion}) are limited to the 25 nodes centered on the current source. The remaining nodes are described by passive cable equations. When the external field is applied to the nerve fiber, the Matlab differential equations solver 'ode45' is used to calculate the membrane voltages $\mathbf{V}_m$. Firing of the fiber is detected by checking whether at least five nodes of Ranvier have membrane voltages greater than 50 mV at any point in time (the resting voltage is approximately -70 mV). Requiring that multiple nodes are firing provides a means of checking that the action potential is propagating to nearby nodes. Plots of the action showed that the signal was propagating away from the stimulus site, as expected.

After the external field is calculated and the nerve model is assembled, the external field is interpolated to the (x,y,z) position of each fiber's nodes of Ranvier. A stimulus response curve is generated by sweeping the excitation current from zero to a maximum value. For each current value, the number of fibers that produce action potentials is noted. Because this process is very computationally intensive, a coarse search is first done to find the current range of interest (i.e. from the current at which the first fiber fires to the current at which the last fiber fires). Once a fiber has fired, it is assumed to be firing at all higher currents and its response is no longer checked.

This procedure produces stimulus response curves in terms of the fraction of fibers firing. Experimentally, the observed CMAP response / muscle twitch is generated when nerve fibers activate individual motor units. The calculation

of CMAP waveforms from nerve fiber potentials is complex. At this point we make the naïve assumption that the measured response is linearly related to the fraction of fibers firing. This can be justified as no CMAP response will be observed before the first nerve fibers begin to fire, and the maximal CMAP is found when all fibers are firing. However, this remains an area for further investigation.

III. RESULTS

A. Model Geometry

An idealized model of a limb was developed using the COMSOL finite element code (COMSOL AB, Stockholm, Sweden) with post-processing done in Matlab (The Mathworks, Natick, MA). The limb was modeled as a homogenous 20 cm long volume with elliptical cross-section (4 cm x 6 cm) as shown in Figure 4. A needle electrode (modeled as a point source) is located inside the limb and injects a current. A 1 cm x 2.1 cm surface electrode is held at ground and provides the return path for the current. A 1 mm thick skin layer surrounds the limb interior, which has the properties of skeletal muscle. Tissue electrical properties are homogenous and frequency-dependent, and are from [8].

Boundary conditions are set so that no current flow is allowed through the skin-air interface. At the ends of the limb (where the model is truncated), the boundaries are held at ground. The point source was assumed to apply square pulses. The input waveform was sampled at 1 MHz, so the Nyquist frequency was 0.5 MHz. This sampling rate was used to give an accurate reconstruction of the waveform. Response for 2.048 msec was calculated, giving 1024 positive FFT bins.
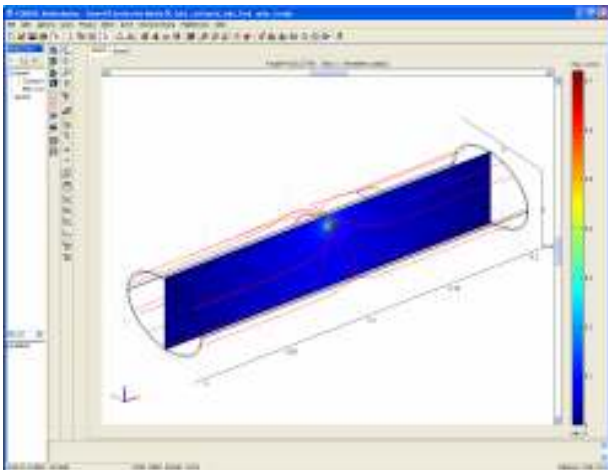
Figure 1: Geometry used in finite element model.

B. Predicted External Field

Figure 2 shows predicted time series created using the iterative procedure outlined above, for the needle positions 3 mm and 8.75 mm from the nerve. A fine frequency sampling

was made consisting of 30 points in frequency from 1 Hz -1 MHz and was used to generate a first set of results; note that the charging/discharging behavior seen at the start and end of the pulse is due to tissue capacitance. The 30 frequencies were downsampled to 15 by discarding alternate points. The 30- and 15-frequency solutions are nearly identical, indicating that the solution has converged with 15 frequency points. Further reducing the number of frequencies to 7 leads to substantial errors. Based on this result, 15 frequency points are used for simulations presented below.
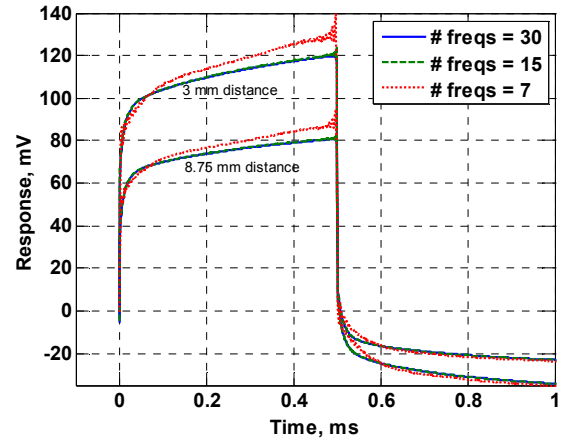
Figure 2. Predicted response to a 0.5 ms pulse at distances 3 mm and 8.75 from the nerve. The interpolation approach is used with 30, 15, and 7 frequencies logarithmically spaced from 1 Hz to 1 MHz. The solution appears to converge as the frequency sampling is increased.

C. Nerve Response

Figure 3 shows computed stimulus-response curves for the overall nerve as a function of stimulus current and needle-to-nerve distance (100 µs pulse width). Some discretization is observed due to the limited number of fibers, but the general trends are clear. A plateau is seen near 45% where all larger fibers are firing but smaller fibers are not yet firing. Near the nerve, threshold currents decrease and the response becomes very sensitive to small changes in stimulus current.
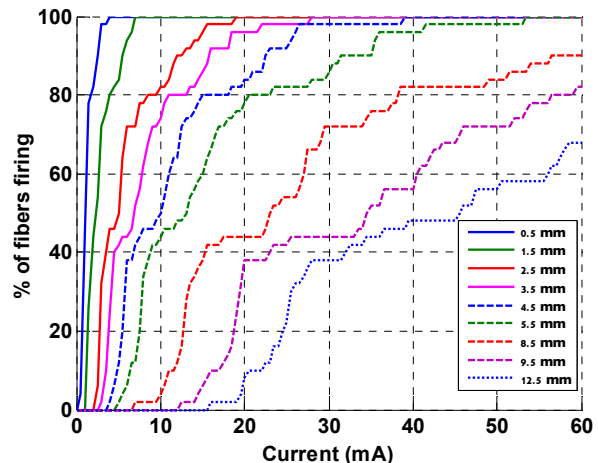
Figure 3. Predicted stimulus response curves (expressed as fraction of fibers firing) vs. needle-to-nerve distance and input current.

D. Use of model output in simulating nerve localization

For predicting CMAP response, the stimulus-response curves shown in Figure 3 were smoothed and scaled to give a maximal response of 5 mV (assuming a linear relationship between CMAP response and the fraction of fibers firing). The CMAP response for any needle distance and stimulus current is then found by interpolating results from Figure 3.

Figure 4 demonstrates a simple PNS scenario. In this procedure the physician sets a target CMAP response of 0.25 mV, which is intended to correspond to a visible muscle twitch. A target current of 0.5 mA is also set.
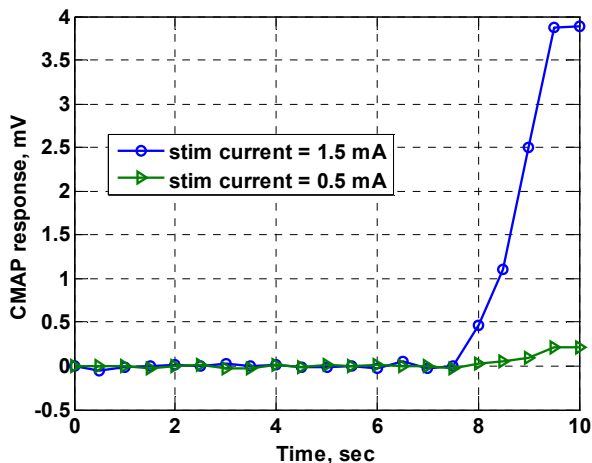
Figure 4. Example PNS procedure. The modeled response is seen while as the needle approaches the nerve at 1 mm/sec from an initial distance of 10 mm. For lower currents, response indicates proximity to the nerve.

In this example, the needle starts 10 mm away from the nerve and is advanced towards the nerve at a rate of 1 mm/sec. Response curves are shown for 1.5 and 0.5 mA stimuli. A CMAP is evoked for the 1.5 mA current at roughly 2.5 mm from the nerve, while a response to the 0.5 mA current is seen at roughly 1 mm from the nerve. In common practice, physicians start with a higher current and manually adjust the current downwards [10]. Initial response to higher currents indicates the needle is approaching the nerve, while the ability to elicit a response at a low current suggests the needle is in close proximity to the nerve.

IV. DISCUSSION

Numerical results above show that the interpolation approach requires approximately 15 frequencies to be calculated in order for results to converge. Run time is approximately 70 sec per frequency, so the use of 15 frequency points is a substantial savings over the 1024 frequency points required for a brute-force calculation.

The stimulus-response curves from Figure 3 show that overall trends can be captured using a relatively small number of nerve fibers. The effect of the multi-modal fiber diameter distribution can also be clearly seen, especially at longer distances where the smaller fibers are not well excited. This highlights the importance of accurate fiber distribution models.

Finally, while the FEM model allows for modeling of realistic anatomy, an idealized anatomy was used for this initial study. Internal tissue structures such as fascial planes can have a noticeable impact on the efficacy of nerve localization and should be included in future work.

V. CONCLUSION

This paper describes a FEM modeling framework for accurately modeling peripheral nerve stimulation in regional anesthesia. The FEM model extends previous PNS simulations by allowing realistic anatomy to be studied. Several enhancements to standard approaches were used for modeling the external field. An interpolation approach was developed that allows the use of realistic frequency-dependent tissue properties without large computational penalty. Numerical results also demonstrated that the exact Helmholtz equation could be solved, rather than quasistatic approximations, without noticeable computational cost. The modeled external field was connected to a Frankenhaeuser-Huxley model for nerve response and used to predict stimulus-response curves as a function of needle position. Finally, the use of the simulator was demonstrated for a simple nerve localization scenario. The simulator provides a useful testbed for better understanding peripheral nerve localization.

REFERENCES

[1] C.R. Johnson, R.C. Barr, and S.M. Klein, "A computer model of electrical stimulation of peripheral nerves in regional anesthesia,", Anesthesiology 106(2), Feb. 2007.

[2] W.F. Urmey and P. Grossi, "The use of sequential electrical nerve stimuli (SENS) for location of the sciatic nerve and lumbar plexus," Regional Anesthesia and Pain Medicine, Vol 31(5), Sept-Oct 2006, pp 463-469.

[3] A.R. Sauter, M.S. Dodgson, H, Kalvoy, S. Grimnes, A. Stubhaug, O. Klasstad, "Current threshold for nerve stimulation depends on electrical impedance of the tissue: a study of ultrasound-guided electrical nerve stimulation of the median nerve", Anesthesia & Analgesia, Vol. 104(4), 2009, pp. 1338-1343.

[4] R. Plonsey, Bioelectric Phenomena, Chapter 5, McGraw-Hill Press, New York, 1969.

[5] N.S. Stoykov, M.M. Lowery, A. Taflove, and T.A. Kuiken, "Frequency- and Time-domain FEM models of EMG: Capacitive effects and aspects of dispersion," IEEE Transactions on Biomedical Engineering, Vol. 49, No. 8, August 2002, pp. 763-772.

[6] C.A. Bossetti, M.J. Birdno, and W.M. Grill, "Analysis of the quasi-static approximation for calculating potentials generated by neural stimulation," J. Neural Eng., Vol 5, 2008, pp. 44-53.

[7] B. Frankenhaeuser and A.L. Huxley, "The action potential in the myelinated nerve fiber of Xenopus Loevis as computed on the basis of voltage clamp data," J. Physiol., Vol 171, 1964, pp 302-315.

[8] C. Gabriel, S. Gabriel and E. Corthout, "The dielectric properties of biological tissues: I. Literature survey", Phys. Med. Biol, Vol. 41, 1996, pp. 2231-2249.

[9] I.A. Boyd and M.R. Davey, Composition of Peripheral Nerves, Edinburgh, E&S Livingston Ltd, 1968

[10] J.D. Vloka, A. Hadzic, H. Shih, D.J. Birnbach, "A national survey on practice patterns in the use of peripheral nerve stimulators in regional anesthesia," The Internet Jour. Of Anesthesiology, Vol 3(4), 1999.